Crystal structure and photocatalytic activity of luminescent 3D-Supramolecular metal organic framework of dysprosium

Sindhu T.K [b], Rani Pavithran [a,*], Sabitha Mohan M.R [b]

[a] Department of Chemistry, College of Engineering Trivandrum, Thiruvananthapuram, Kerala, India
[b] Department of Chemistry University College Thiruvananthapuram, Kerala, India

ARTICLE INFO

ABSTRACT

A 3D supramolecular metal organic framework of dysprosium has been fabricated through a facile hydrothermal procedure with the ligand, 2,6-naphthalene disulphonic acid and the co-ligand, 4,4′-bipyridine. The MOF has been characterized as $[C_{60}H_{81}DyN_8O_{30}S_4]$ by routine analytical procedures. SXRD studies of the MOF show the existence of a hydrogen-bonded 3D supramolecular structure with high porosity. It crystallizes in monoclinic space group $P2_1/n$ with unit cell parameters, a = 16.5424(6) Å, b = 37.0052(14) Å, c = 24.4361(9) Å, β = 100.7410°, α = γ = 90°. The Dy-MOF has eight coordinated water molecules around the metal centre and exhibits square anti-prismatic geometry. The band gap is 3.11 eV. The degradation experiments under visible light confirmed that Dy-MOF can act as a photocatalyst. Addition of hydrogen peroxide remarkably increases the degradation efficiency of the MOF through an advanced oxidation process. The newly synthesized MOF produced sharp emission peaks characteristic of dysprosium ion.

1. Introduction

Photocatalysis is an efficient way of environment-friendly transformation of renewable energy. The photocatalytic activity by MOF is a challenging field in which a plethora of research is still going on to develop suitable catalysts to attain the goals of sustainable development. Key factors such as favourable band gap, porosity, available adsorption sites and thermal as well as chemical stability made the selected MOFs highly adaptable in photocatalysis [1–17].

One of the adverse effects of industrialization is fresh water contamination by toxic chemicals, dyes, and other effluents. In this scenario, the emergence of MOF as a visible-light catalyst for dye degradation is more relevant. Recently, dye degradation efficiency of a number of MOFs has been studied in water [17–23].

Lanthanide based metal organic frameworks (Ln-MOF) have desirable emission properties like high quantum yield and sharp line emissions characteristic of the metal ion. The luminescence intensity is responsive to the coordination environment making them suitable for sensor applications. Combination of the special properties of lanthanides and the advantages of MOFs make Ln-MOFs promising for specific applications.

Thus we have synthesized the MOF of the lanthanide, dysprosium, with a view to investigate its single crystal structure, its photocatalytic efficiency in the removal of methylene blue, and its stability and reusability. Sodium salt of 2,6-naphthalenedisulfonic acid (2,6-NDS) was used as the ligand and 4,4′-bpy was used as the co-ligand. Hydrogen peroxide increases the catalytic activity by the

---

advanced oxidation process (AOP). Six oxygen atoms on the sulfonate groups of the ligand act as H-bonding acceptor, which facilitate the formation of 3D supramolecular architectures [24–26].

2. Experimental section

2.1. Materials and Techniques

A.R grade chemicals purchased were utilized as such without further treatment. The same instruments as reported [27] have been used for the synthesis, FT-IR analysis, TGA, Powder X-ray diffraction studies, and for fluorescence spectral studies.

2.2. Synthesis of Dy-MOF

1 mmol $Dy(NO_3)_3.6H_2O$, 2 mmol sodium salt of 2,6-NDS and 2.1 mmol 4,4′-bipyridine (bpy) were mixed with 10 mL double distilled water [19,27]. It is then taken in an autoclave and heated at 180 ° under autogenous pressure for three days. It was cooled, filtered, and dried in air.

2.3. SXRD studies

The SXRD data were collected using monochromatic Mo Kα radiation ($\lambda = 0.71073$ Å) at 293 K on a Brucker AXS Kappa APEX ll CCD detector. The structures were solved by direct method and refined by full matrix least squares method on F^2 using SHELXS 2014 and SHELXL 2014 programmes. The CCDC number is 1817702 (Dy-MOF). Structures showing the packing were collected using Diamond software. Mercury software was used to generate structures showing the H-bonds and π-π interactions.

2.4. Dye degradation experiments

A beaker containing 5 mg of MOF and 50 ml of 10 ppm of dye, was kept at 10 cm from the light source, 100 MW xenon lamp. It was stirred in the dark for 1 h to attain adsorption-desorption equilibrium, before light irradiation. The mixture was irradiated with photons of energy higher than the band gap of MOF [17,18,27,28]. Stirring was maintained throughout the experiment. UV–Visible spectra were taken with samples collected at regular intervals, at $\lambda = 664$ nm, wavelength of maximum absorption of the dye. Investigation was also carried out with a mixture of 5 mg MOF, 3.9 %, 300 μL H_2O_2 and 50 ml of 10 ppm MB solution. The UV–visible spectra were taken at different time intervals at 664 nm.

2.5. Leaching experiments

Here, the variation of stability was investigated with pH of the solution, using a mixture of the same quantity of the MOF and dye as used in 2.4, with stirring for 30 min. The change in color with p^H was monitored [29–31].

2.6. Trapping experiments

This is employed for finding the radicals producing the degradation of the dye and thus the mechanism involved. This is done by adding tertiary butyl alcohol (TBA), benzoquinone (BQ), and ammonium oxalate (AO). They are the scavengers for hydroxyl radicals, superoxide radicals, and for leaving holes respectively [21,23,32].

2.7. Recycling experiments

The reusability of the compound was assessed using recycling experiments. The residue was washed with ethanol, water and utilized in the next cycle [33].

3. Results and discussion

3.1. FT-IR spectral analysis

FT-IR spectrum of 2,6-NDS shows the peaks as reported [27] (Fig. S1). The v_{as} and v_s of the SO_3^- groups are at 1260-1183 (v_{as}) and 1100-1034 (v_s) cm^{-1}, respectively, in the MOF (Fig. S2). The small shift shows the absence of direct interaction of metal to the ligand as depicted by SXRD. There exists weak H-bond & pi-pi interaction in the crystal structure. The broad band around 3500-3100 cm^{-1} confirms coordinated water molecules in the MOF, as also evidenced by SXRD.

3.2. Energy Dispersive X ray spectral studies

The purity and compositions of the Dy-MOF was confirmed by EDS analysis. The EDS displays the main elemental peaks of Dy, S and O (Fig. S3, Table S1).

3.3. SXRD of Dy-MOF

The stoichiometry of the newly synthesized Dy-MOF was obtained as $C_{60} H_{81} Dy N_8 O_{30} S_4$ [Dy(H$_2$O)$_8$](4,4'bpy)$_4$(2,6-NDS)(2,6-NDSH)] from SXRD. The MOF was crystallised in the monoclinic space group P2$_1$/n. Each unit was associated with ten lattice water molecules. Eight such units are grouped to form the unit cell, with a = 16.5424(6) Å, b = 37.0052(14) Å, c = 24.4361(9) Å, β = 100.7410°, α = γ = 90° (Tables S2, S3, S4 & S5). The SXRD studies revealed the porous 3D supramolecular structure.

The M − O bonds of length ranging from 2.347 to 2.463 Å around the Dy(III) centres suggest that there are eight coordinated water molecules. The O-Dy-O bond angle suggests a square antiprism geometry around the metal centre, with a coordination environment as shown in Fig. 1.

Absence of Dy–N bonds in the crystal data rule out the direct interaction between the metal centre and the bipyridyl nitrogen. The coordinated water molecules are orienting in such a way as to make strong hydrogen bonds with lattice water, nearest bipyridyl nitrogen and naphthalene disulphonic acid units.

The naphthalene-2,6-disulphonate molecules are aligned parallel and interlink [Dy(H$_2$O)$_8$]$^{3+}$ polyhedra via H-bonding at both sulphonic acid groupings [Fig. S4]. Such assembly is further tailored strongly via H-bonding involving lattice water. The bipyridyl molecules are aligned in planes almost perpendicular to the plane of NDS. The bipyridyl molecules interlink the [Dy(H$_2$O)$_8$]$^{3+}$ units by H-bonding between the nitrogen on both rings and coordinated water molecules. Fig. S5 shows the H-bonding interaction between [Dy(H$_2$O)$_8$]$^{3+}$ and bipyridine. This kind of extensive H-bonding involving the coordination polyhedra [Dy(H$_2$O)$_8$]$^{3+}$, 4,4'-bipyridine and 2,6-napthalene disulphonic acid and lattice water molecules make a highly porous three dimensional supramolecular architecture (Fig. 2). Packing along different axes is shown in Figs. S6 and S7 respectively.

3.4. Powder XRD studies

Powder XRD experiments were performed for confirming the phase purity of Dy-MOF. Sharp peaks show that the MOF is crystalline [Fig. 3]. The formation of nano crystals was confirmed by the crystallite size 67 nm obtained from Scherrer equation.

3.5. BET surface area of Dy-MOF

Nitrogen adsorption-desorption experiments were done at −195 °C and the curve [Fig. S8] shows a Type lV adsorption with a hysteresis loop [34,35]. The average pore diameter is 18.70 nm which corresponds to mesopore type. BET surface area is 2.2960 m^2/g. At very low relative pressure the adsorption isotherm shows a plateau and a very slow stepping up at 0.62p/p^0 indicating the filling of nitrogen [36]. The isotherm goes up steeply after 0.82p/p^0 and reaches a maximum adsorption of 10 cm^3/g. This is an indication of adsorption of more nitrogen & some mesopore is formed by powder interspace of the dehydrated material. The adsorption curve coincides with the desorption curve at 0.5 p/p^0 showing that the framework is very stable.

3.6. Thermogravimetric analysis

The stability of Dy-MOF, {[Dy(H$_2$O)$_8$] (NDS)(NDSH)(bpy)$_4$}.10H$_2$O was analyzed by performing TG and DTG [Fig. S9]. The first stage of its decomposition was from 80° to 140° C and the observed weight loss is 4.0 %. This is due to the removal of four lattice H$_2$O (among the ten water molecules) for which the estimated weight loss was 4.27 %. The six lattice water molecules remain stable due to hydrogen bonding with 2,6-NDS and 4,4'-bpy in the framework. The decomposition of water continued in the next stage till 230° C. The weight loss, corresponding to this change was 15.08 %, which agreed with the calculated weight loss of 14.95 % due to 14 water
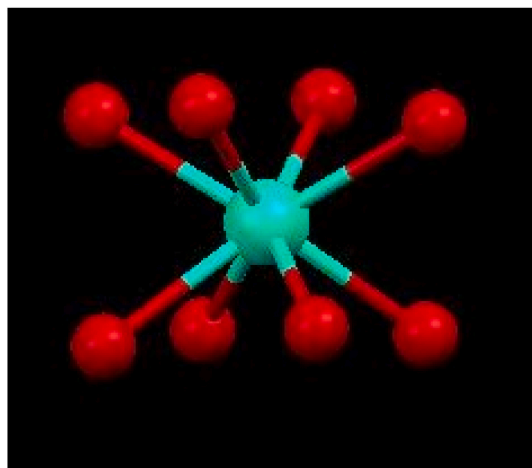
Fig. 1. Octa coordinated Dy^{3+}.
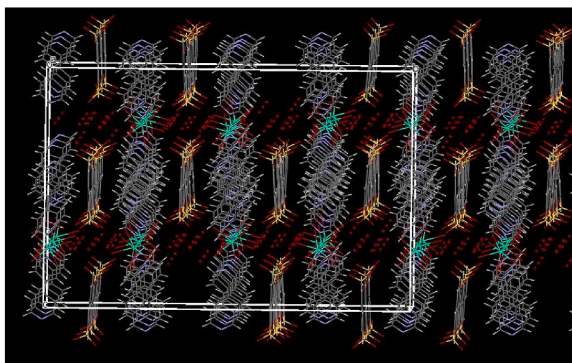
Fig. 2. 3 D view of the MOF.
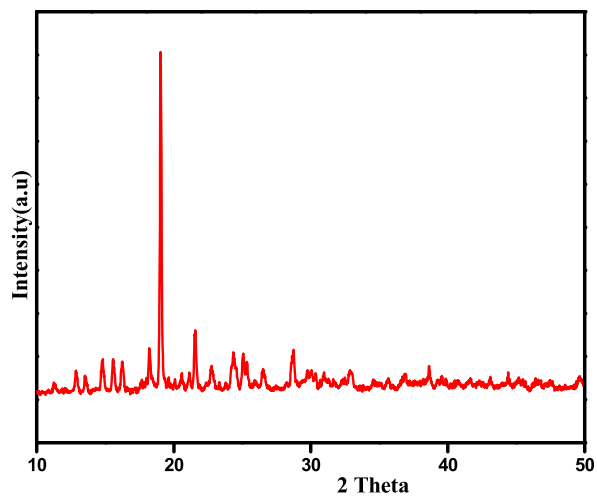
Fig. 3. Pxrd of Dy-MOF.
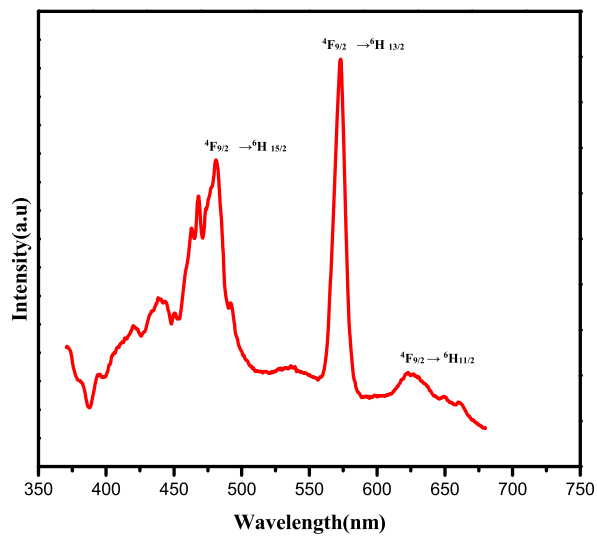
Fig. 4. The Emission spectrum of Dy-MOF.

molecules; 6 lattice and 8 coordinated water molecules. The anhydrous system thus formed, decomposed gradually from 230 ° C to 545° C, amounting to a loss of 37.0 %, which can be due to the removal of four bipyridines and it matches well with the calculated weight loss of 37.03 %. The final decomposition was from 545 ° C to 650 ° C. This may be due to the complete loss of two naphthalene disulphonic acids and the residue left behind was Dy_2O_3. The weight of the residue was 15 % which agrees with 14.08 %, the calculated value. The thermal behaviour of Dy-MOF is in agreement with the SXRD structure.

3.7. Photoluminescence studies

Solid-state excitation (Fig. S10) and emission spectra (Fig. 4) of Dy-MOF were collected at room temperature. The excitation spectrum of Dy-MOF is monitored at 573 nm around the intense $^4F_{9/2} \rightarrow ^6H_{13/2}$ transition of Dy^{3+} ion. The π-π* transition of the ligand is indicated by the broad band in 250–350 nm in the excitation spectrum. A less intense, weak band is also seen in the 350–450 nm region. The absence of absorptions corresponding to the transitions between the energy levels of the metal ions shows the efficiency of antenna effect in MOFs.

When excited at 330 nm, Dy-MOF shows three characteristic emission bands centered at 491 nm, 572 nm and 632 nm, due to the emissions $^4F_{9/2} \rightarrow ^6H_J$ (J = 15/2, 13/2 and 11/2) of Dy^{3+} ion. The most intense peak is at 572 nm of $^4F_{9/2} \rightarrow ^6H_{13/2}$ [36] with a quantum yield 1.47 and CIE coordinate (0.37147, 0.56311) (Fig. S11). The peaks due to the ligands are absent in the spectrum, which may be due to the antenna effect [37,38].

3.8. UV-Diffuse Reflectance spectral studies

UV-DRS spectrum of Dy-MOF is depicted in Fig. S12. The band gap was (Fig. 5) calculated from Tauc's plot and is found to be 3.11 eV, which suggests that the Dy-MOF is a suitable candidate for photocatalytic applications [39].

3.9. Photocatalytic activity of Dy-MOF

The degradation experiments were performed under visible light in an aqueous solution in the absence [Fig. S13] and presence of hydrogen peroxide [Fig. S14] as explained in 2.4. The photo degradation was negligible in the absence of Dy-MOF.

The photo degradation of MB is quantified in Fig. 6. From the graph it is clear that 58 % of MB was degraded within 50 min without hydrogen peroxide. And almost 93 % of the dye was degraded within 25 min using hydrogen peroxide.

The mechanism of photo catalysis without H_2O_2 is different from that in the presence of H_2O_2. When Dy-MOF was exposed to photons with energy greater than 3.11eV, electrons get excited from the valence band (VB), thus holes were formed [40,41]. The holes in the excited state act as strong oxidants and oxidises the dye, resulting in 58 % of degradation in 50 min. However, in presence of H_2O_2 the degradation rate is very high, due to the advanced oxidation process (AOP) [41–43], owing to the high activity of hydroxyl radical obtained from H_2O_2 [40,41]. Moreover, H_2O_2 suppresses the electron-hole pair recombination, acting as an electron acceptor. Hence, the Dy-MOF is a better photo catalyst with H_2O_2.

The kinetics of the photo degradation was investigated by fitting the experimental data in a first order model using the Langmuir-Hinshelwood equation [Tables S6 and S7]. Fig. S15 shows a linear relationship between $\ln(C/C_0)$ and the time of degradation (t) of MB, as in $\ln C/C0 = -kt$, where C0 and C are the initial concentration and concentration at time t and k is the rate constant. The value of k is 4 * 10-2 in presence of H2O2 and k has a value of 1.06 * 10-3 without H2O2 [Figs. S15 and S16] [31,42–45].
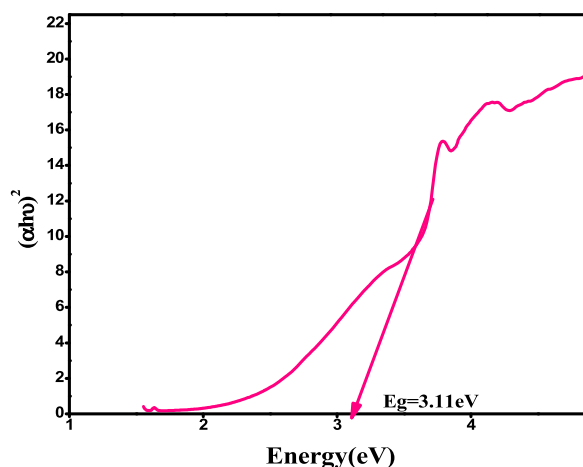
Fig. 5. Tauc's plot and Band Gap of Dy-MOF.
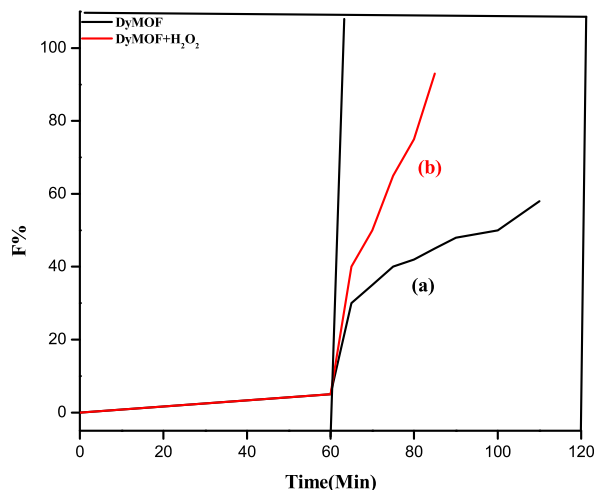
Fig. 6. Degradation of MB (a) with Dy MOF alone and (b) in presence of Dy MOF and Hydrogen peroxide.

3.10. Leaching experiments

Leaching experiments were conducted as in 2.5. The colour was monitored at different p^H at regular intervals. There was no colour change at low p^H and only a slight colour change at high pH. At a fixed pH, after the leaching, there was no colour change even though the irradiation was continued. This leaching experiment reveals the effectiveness of the Dy-MOF as a non leaching photocatalyst for the dye degradation of methylene blue [Fig S 17] [29–31].

3.11. Trapping experiments

Trapping experiments were performed as in 2.6 [21,23,32]. The degradation was found to be 38 %, 80 % and 35 % respectively, on adding 5 mmol of scavengers, TBA, BQ and AO to MB. Since the addition of TBA and AO reduces the rate of degradation, hydroxyl radicals and holes are responsible for the degradation of methylene blue [Fig. 7]. Both these radical scavengers have quenched the reaction to the same degree [Fig. S18].

3.12. Reusability and stability of Dy-MOF as a photocatalyst

Recyclability is decisive in the applicability of photocatalysts. The reusability of Dy-MOF was assessed through recycling experiments (section 2.7). Even after five cycles, the photocatalytic efficiency decreases from 95 % to only 90 %. There is no loss in the activity of MOF in the dye degradation which proves the reusability of Dy-MOF [Fig. S19]. It is evident that the MOF was active even after five cycles [22,23,33,44].

Phase purity of the compound is indicated by the agreement between major peaks in the PXRD of the as synthesized MOF and of the simulated one in SXRD [Fig. 8]. The stability of Dy-MOF was confirmed by the similarity in the peaks observed after degradation experiments with that of as synthesized pattern.

Soaking experiments were also performed to assess the chemical stability of Dy-MOF [22] and PXRD were taken before and after the soaking experiments and were compared [Fig. 8]. No remarkable change was noticed. This illustrates the chemical stability of Dy-MOF. Stability and reusability are essential for photo catalysts to be used for industrial applications.

The infrared spectrum of the as synthesized Dy-MOF was compared with that of the MOF obtained after the dye degradation experiment [Fig. 9]. IR showed similar peaks, confirming its stability. Thus, the results confirmed the stability and reusability of the newly synthesized MOF in the removal of methylene blue dye, a carcinogenic pollutant from wastewater.

The degradation efficiency of DyMOF was compared with that of similar compounds in the literature and is given in Table 1. The Dy MOF is more efficient when compared to others, as an appreciable degradation has been achieved with less quantity of the photocatalyst and for a lower time of irradiation.

4. Conclusion

3D supramolecular metal organic framework of dysprosium was synthesized using 2,6-NDS and 4,4' bpy through a facile hydrothermal route. The SXRD data confirmed high degree of crystallinity of the MOF. The MOF is present in the nano regime and band gap energy is 3.11 eV. The photocatalytic efficiency of the as prepared Dy-MOF has been demonstrated in the degradation of MB. The mechanistic steps have been investigated and reusability as well as chemical stability was tested. In the presence of H_2O_2, the degradation proceeds through advanced oxidation process (AOP). Dy-MOF is luminescent due to the Dy^{3+} ion. The Dy MOF is an
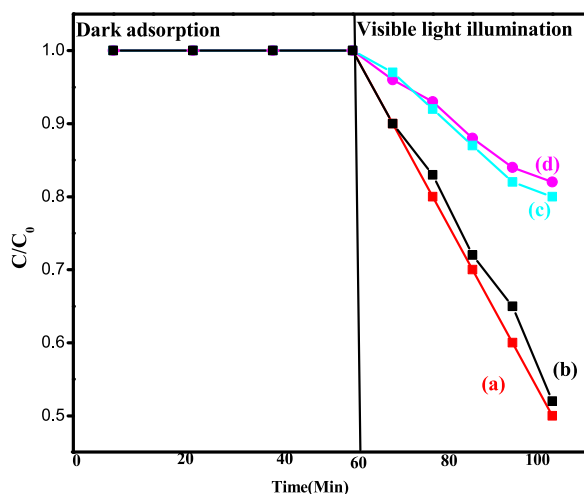
Fig. 7. Effect of radical scavengers (a) MB (b) BQ (c) AO and (d) TBA on MB decolorization in the presence of Dy-MOF.
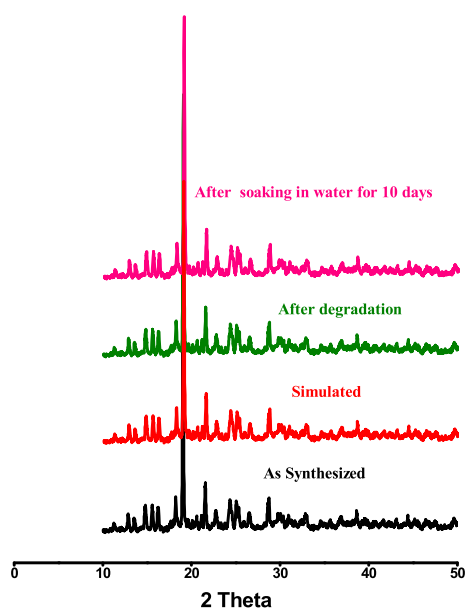
Fig. 8. PXRD Patterns of different samples of Dy-MOF - as Synthesized, Simulated, after Degradation and after soaking in water for 10 days.

efficient photocatalyst, when compared to other lanthanide MOFs in dye degradation in terms of less quantity of the photocatalyst and for a lower time of irradiation.

The X-ray crystallographic data of $[Dy(H_2O)_8(NDS)(NDSH)(bpy)_4].10H_2O$ was deposited in CCDC as supplementary data **(CCDC NO 1817702)** and available free of charge via http://www.ccdc.ac.uk/conts/retrieving.html, or from the Cambridge Crystallographic Data Centre, 12 Union Road, Cambridge CB2 IEZ, UK, Fax: (+44)1223-336-033 or e-mail:deposit@ccdc.cam.ac.uk. In the supplementary information IR Spectra, EDAX and TG & DTA are included.

CRediT authorship contribution statement

Sindhu T.K: Investigation, Writing – original draft, Resources, Validation. **Rani Pavithran:** Conceptualization, Supervision, Writing – review & editing, Methodology. **Sabitha Mohan M.R:** Writing – original draft, Investigation, Resources.

Declaration of competing interest

The authors declare that they have no known competing financial interests or personal relationships that could have appeared to
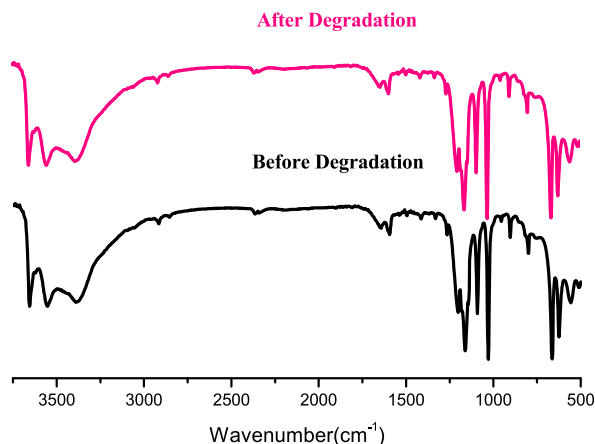
Fig. .9. Ir spectra of Dy-MOF before degradation and after degradation.

Table 1
Photo degradation efficiency of different lanthanide MOFs-a comparison.

Photocatalyst	Source	Pollutant	Initial Concentration (mg/l)	Irradiation time(min/h)	Efficiency (%)	References
Tb-MOF	UV	RhB	20	6 h	96	[46]
Eu-MOF	UV	RhB	20	6 h	94	[46]
$Eu_{0.01}Tb_{0.09}$-MOF	UV	RhB	20	6 h	65	[46]
Nd-MOF	UV	MV	50	40	65.7	[22]
La-BDC + H_2O_2	Visible	RhB	30	2h	69.47	[47]
La-NDC + H_2O_2	Visible	RhB	30	2h	89.3	[47]
La-BDC	UV	RhB	128	2h	5.7	[47]
La-NDC	UV	RhB	128	2h	18.32	[47]
La-PTC	Visible	MB	10	4h	64.07	[48]
$[Dy(H_2O)_8(NDS)(NDSH)(bpy)_4].10H_2O$	Visible	MB	10	50 min	58	Present work
$[Dy(H_2O)_8(NDS)(NDSH)(bpy)_4].10H_2O +$ H_2O_2	Visible	MB	10	25 min	93	Present work

influence the work reported in this paper.

Appendix A. Supplementary data

Supplementary data to this article can be found online at https://doi.org/10.1016/j.heliyon.2023.e21262.

References

[1] F. Saraci, V.Q. Novo, P.R. Donnarumma, A.J. Howarth, Rare-earth metal-organic frameworks: from structure to applications, Chem. Soc. Rev. 49 (2020) 7949–7977, https://doi.org/10.1039/d0cs00292e.

[2] Y.J. Cui, B.L. Chen, G.D. Qian, Lanthanide metal-organic frameworks for luminescent sensing and light-emitting applications, Coord. Chem. Rev. 273 (2014) 76–86, https://doi.org/10.1016/j.ccr.2013.10.02.

[3] O.M. Yaghi, M.O. Keeffe, N.W. Ockwig, H.K. Cha, M. Eddaoudi, J. Kim, Reticular synthesis and the design of new materials, Nature 423 (2003) 705–714, https://doi.org/10.1038/nature01650. PMID: 12802325.

[4] O.M. Yaghi, Reticular chemistry—construction, properties, and precision reactions of frameworks, J. Am. Chem. Soc. 138 (2016) 15507–15509, https://doi.org/10.1021/jacs.6b11821.

[5] H. Furukawa, N. Ko, Y.B. Go, N. Aratani, S.B. Choi, E. Choi, A.O. Yazaydin, R.Q. Snurr, M. O'Keeffe, J. Kim, O.M. Yaghi, Ultrahigh porosity in metal-organic frameworks, Science 329 (2010) 424–428, https://doi.org/10.1126/science.1192160.

[6] I.M. Hönicke, I. Senkovska, V. Bon, I.A. Baburin, N. Bönisch, S. Raschke, J.D. Evans, S. Kaskel, Balancing mechanical stability and ultrahigh porosity in Crystalline framework materials, Angew. Chem. Int. Ed. 57 (2018) 13780–13783, https://doi.org/10.1002/anie.201808240.

[7] Z. Chen, P. Li, R. Anderson, X. Wang, X. Zhang, L. Robison, L.R. Redfern, S. Murine, T. Islamoglu, D.A.G. Gualdrón, T. Yildirim, J.F. Stoddart, O.K. Farha, Balancing volumetric and gravimetric uptake in highly porous materials for clean energy, Science 368 (2020) 297–303, https://doi.org/10.1126/science.aaz8881.

[8] P. Li, N.A. Vermeulen, C.D. Malliakas, D.A. Gomez- Gualdrón, A.J. Howarth, B.L. Mehdi, A. Dohnalkova, N.D. Browning, M.O. 'Keeffe, O.K. Farha, Bottom-up construction of a superstructure in a porous uranium-organic crystal, Science 356 (2017) 624–627, https://doi.org/10.1126/science.aam7851.

[9] D.X. Xue, Y. Belmabkhout, O. Shekhah, H. Jiang, K. Adil, A.J. Cairns, M. Eddaoudi, Tunable rare earth fcu-MOF platform: access to adsorption kinetics driven gas/vapor separations via pore size contraction, J. Am. Chem. Soc. 137 (2015) 5034–5040, https://doi.org/10.1021/ja5131403.

[10] L.J. Murray, M. Dinca, J.R. Long, Hydrogen storage in metal- organic frameworks, Chem. Soc. Rev. 38 (2009) 1294–1314, https://doi.org/10.1039/b802256a.

[11] L.E. Kreno, K. Leong, O.K. Farha, M. Allendorf, R.P. Van Duyne, J.T. Hupp, Metal–organic framework materials as chemical sensors, Chem. Rev. 112 (2012) 1105–1125, https://doi.org/10.1021/cr200324t.

[12] K. Otake, Y. Cui, C.T. Buru, Z. Li, J.T. Hupp, O.K. Farha, Single-atom-based vanadium oxide catalysts supported on metal–organic frameworks: selective alcohol oxidation and structure-activity relationship, J. Am. Chem. Soc. 140 (2018) 8652–8656, https://doi.org/10.1021/jacs.8b05107.

[13] Y. Cui, Y. Yue, G. Qian, B. Chen, Luminescent functional metal–organic frameworks, Chem. Rev. 112 (2012) 1126–1162, https://doi.org/10.1021/cr200101d.

[14] A.J. Howarth, Y. Liu, J.T. Hupp, O.K. Farha, Metal-organic frameworks for applications in remediation of oxyanion/cation-contaminated water, CrystEngComm 17 (2015) 7245–7253, https://doi.org/10.1039/C5CE01428J.

[15] P. Horcajada, C. Serre, G. Maurin, N.A. Ramsahye, F. Balas, M. Vallet- Regí, M. Sebban, F. Taulelle, G. Férey, Flexible porous metal-organic frameworks for a controlled drug delivery, J. Am. Chem. Soc. 130 (2008) 6774–6780, https://doi.org/10.1021/ja710973k.

[16] M. Kurmoo, Magnetic metal-organic frameworks, Chem. Soc. Rev. 38 (2009) 1353–1379, https://doi.org/10.1039/B804757J.

[17] S. Liu, C. Zhang, Y. Sun, Q. Chen, L. He, K. Zhang, J. Zhang, B. Liu, L.F. Chen, Design of metal-organic frameworks-based photocatalysts for hydrogen generation, Coord. Chem. Rev. 413 (2020) 213–266, https://doi.org/10.1016/j.ccr.2020.213266.

[18] A. Fateeva, P.A. Chater, C.P. Ireland, A.A. Tahir, Y.Z. Khimyak, P.V. Wiper, J.R. Darwent, M.J. Rosseinsky, A water-stable porphyrin-based metal-organic framework active for visible-light photocatalysis, Angew. Int. Ed. (2012) 517440–517444, https://doi.org/10.1021/anie.20120247.

[19] C.Y. Lee, O.K. Fatha, B.J. Hong, A.A. Sergeants, S.T. Nguyen, J.T. Hupp, Light harvesting metal-organic frameworks (MOFs): efficient strut-to-strut energy transfer in bodipy and porphyrin-based MOFs, J. Am. Chem. Soc. 40 (2011) 15858–15861, https://doi.org/10.1021/ja206029a.

[20] J. Wang, C. Rao, L. Lu, S. Zhang, M. Muddassir, J. Liu, Efficient Photocatalytic degradation of methyl violet using two new 3D MOFs directed by different Carboxylate Spacers, CrystEngComm (2021) 23741–23747, https://doi.org/10.1039/d0ce01632b.

[21] S. Jensen, K. Tan, W. Lustig, D. Kilin, J. Li, Y. J Chabal, T. Thonhauser, Quenching of photoluminescence in a Zn-MOF sensor by nitroaromatic molecule, J. Mater. Chem. C 7 (2019) 2625–2632, https://doi.org/10.1039/C8TC06281A.

[22] I.J. Kang, N.A. Khan, E. Haque, S.H. Jhung, Chemical and thermal stability of isotypic metal-organic frameworks: effect of metal ions, Chem. Eur J. 17 (2011) 6437–6442, https://doi.org/10.1002/chem.201100316.

[23] T. Minh, N.T.T. Tu, T.T. Van Thi, L.T. Hoa, H.T.L. Nguyen, H. Phong, T.L.M. Pham, Q. Khieu, Synthesis of porous octahedral ZnO/CuO composites from Zn/Cu based MOF-199 and their applications in visible-light –driven photocatalytic degradation of dyes, J. Nanomater. (2019) 179–183, https://doi.org/10.1155/2019/5198045.

[24] O.K. Farha, I. Eryazici, N.C. Jevon, B.G. Hauser, C.E. Wilmer, A.A. Sarjeant, R.Q. Snurr, S.T. Nguyen, A.O. Yazaydin, J.T. Hupp, Metal-organic frameworks materials with ultrahigh surface areas: is the Sky the Limit? J. Am. Chem. Soc. (2012) 1–7, https://doi.org/10.1021/ja3055639.

[25] J.M. Li, R. Huo, X. Li, H.L. Sun, Lanthanide-organic frameworks constructed from 2,7-naphthalene disulfonate and 1H-imidazole[4,5-f][1,10]- phenanthroline: synthesis, structure, and luminescence with near–visible light excitation and magnetic properties, Inorg. Chem. 58 (2019) 9855–9865, https://doi.org/10.1021/acs.inorgchem.9b00925.

[26] J. Perles, N. Snejko, M. Iglesias, M.A. Monge, 3D Scandium and yttrium arenedisulphonates MOF materials as highly thermally stable bifunctional heterogeneous catalysts, J. Mater. Chem 10 (2009) 6504–6511, https://doi.org/10.1039/b902954k.

[27] T.K. Sindhu, R. Pavithran, A. Vidhya, Design of 3D-supramolecular metal organic framework of zinc as photocatalyst for the degradation of methylene blue through advanced oxidation process, J.Mol.Struct. 1245 (2021), 131039.

[28] N. Daneshvar, D. Salari, A.R. Khataee, Photocatalytic degradation of azo dye acid red 14 in water on ZnO as an alternative catalyst to TiO2, J. Photochem. Photobiol., A : Chemistry 162 (2004) 317–322, https://doi.org/10.1016/S1010-6030(03)00378-2.

[29] L.M. Zhao, W.T. Zhang, K.Y. Song, Q.Q. Wu, Y. Li, H.H. Li, Z.R. Chen, Lead-carboxylate/polyiodide hybrids constructed from halogen bonding and asymmetric viologen: structures, visible-light-driven photocatalytic properties and enhanced photocurrent responses, CrystEngComm 20 (2018) 2245–2252, https://doi.org/10.1039/C8CE00120K.

[30] V. Au, Recent Advances in the use of metal-organic frameworks for dye adsorption, Front. Chem. 8 (2020) 708, https://doi.org/10.3389/fchem.2020.00708.

[31] R. Abazari, S. Sanati, A. Morsali, A.M. Kirillov, A.M.Z. Slawn, C.L.C. Warren, Simultaneous presence of open metal sites and amine groups on a 3D Dy (III) metal-organic framework catalyst for mild and solvent free conversion of CO2 to cyclic carbonates, Inorg. Chem. 60 (3) (2021) 2056–2067, https://doi.org/10.1021/acs.inorgchem.0c03634.

[32] J.L. Wang, L.J. Xu, Advanced oxidation processes for wastewater treatment: formation of hydroxyl radical and application, Crit. Rev. Environ. Sci. Technol. 42 (2012) 251–325, https://doi.org/10.1080/10643389.2010.507698.

[33] Y. Yang, W. Wang, H. Li, X. Jin, H. Wang, L. Zhang, Y. Zhang, NH2-MIL-53(Al) nano crystals anchored on the surface of RGO hollow spheres and its visible light degradation of methylene blue, Mater. Lett. 197 (2017) 17–20, https://doi.org/10.1016/j.matlet.2017.03.041.

[34] P. Herman, I. Fabian, J. Kalmar, Mesoporous silica-gelatin aerogels for the selective adsorption of aqueous Hg(II), ACS Appl. Nano Mater. 3 (2020) 195–206, https://doi.org/10.1021/acsanm.9b01903.

[35] F. Tian, J. Xiong, H. Zhao, Y. Liu, S. Xiao, R. Chen, Mannitol-assisted solvothermal synthesis of BiOCl hierarchical nanostructures and their mixed organic dye adsorption capacities, CrystEngComm 16 (2014) 4298–4305, https://doi.org/10.1039/c4ce00160e.

[36] S. Kitagawa, R. Kilaura, S.I. Noro, Functional porous coordination polymers, Angew. Chem. Int. Ed. 43 (2004) 2334–2375, https://doi.org/10.1002/anie.200300610.

[37] Z.Q. Jiang, G.Y. Jiang, D.C. Hou, F. Wang, Z. Zhao, J. Zhang, Urothermal synthesis of the photoluminescent lanthanide-organic framework with unusual topologies, CrystEngComm 15 (2013) 315–323, https://doi.org/10.1039/C3CE26242H.

[38] S. Sivakumar, M.L.P. Reddy, A.H. Cowley, K.V. Vasudevan, Synthesis and crystal structures of lanthanide 4-benzyloxy benzoates: influence of electron-withdrawing and electron-donating groups on luminescent properties, Dalton Trans. 39 (2010) 776–786, https://doi.org/10.1039/B917256D.

[39] M. Zhang, L. Wang, T. Zeng, Q. Shang, H. Zhou, Z. Pana, Q. Cheng, Two pure MOF-Photocatalysts with ready preparing for the degradation of methylene blue under visible light, Dalton Trans. 47 (2018) 4251–4258, https://doi.org/10.1039/C8DT00156A.

[40] E. Ortiz, C.V. Gómez, C.M. Cortés-Romero, H. Solís, R. Ruiz-Ramos, S. Loera-Serna, Degradation of indigo carmine using advanced oxidation processes: synergy effects and toxicological study, J. Environ. Protect. 7 (2016) 1693–1706, https://doi.org/10.4236/jep.2016.712137.

[41] M. Zhang, R. Luo, C. Wang, W. Zhang, X. Yan, X. Sun, L. Wang, J. Li, Confined pyrolysis of metal-organic frameworks to N-doped hierarchical carbon for non-radical dominated advanced oxidation process, J. Mater. Chem. A 7 (2019) 12547–12557, https://doi.org/10.1039/C9TA02931A.

[42] Z.J. Xie, Y.P. Feng, F.L. Wang, D.N. Chen, Q.X. Zhang, Y.Q. Zeng, Construction of carbon dots modified MoO3/g-C3 N4 Z-scheme photocatalyst with enhanced visible light photocatalytic activity for the degradation of tetracycline, Appl. Catal. B Environ. 229 (2018) 96–104, 10.1016/S1872-2067-2067(19) 63391-7.

[43] R. Hailili, Z.Q. Wang, Y.X. Li, Y.H. Wang, V.K. Sharma, X.Q. Gong, Oxygen vacancies induced visible light photocatalytic activities of CaCu3Ti4O12 with controllable morphologies for antibiotic degradation, Appl. Catal. B Environ. 221 (2018) 422–432, https://doi.org/10.1016/j.apcatb.2017.09.026.

[44] M. Waqar, M. Imran, S. Farooq, A.S. Noreen, S. Latif, M. Khan, M. Rafiq, H. Siddiqui, Enhanced photoluminescence and photocatalytic efficiency of La-doped bismuth molybdate: its preparation and characterization, Materials 13 (2020) 1–12, https://doi.org/10.3390/ma13010035.

[45] H.P. Jing, C.C. Wang, Y.W. Zhang, P. Wang, R. Li, Photocatalytic degradation of methylene blue in ZIF-8, RSC Adv. 4 (2014) 54454–54462, https://doi.org/10.1039/C4RA08820D.

[46] F. Wang, Y. Pu, X. Zhang, F. Zhang, H. Cheng, Y. Zhao, A series of multifunctional lanthanide metal-organic frameworks for luminescence sensing and photocatalytic applications, J. Lumin. 206 (2019) 192–198, https://doi.org/10.1016/j.jlumin.2018.10.061.

[47] A. Buhari, A. Zulys, J. Gunlazuardi, Synthesis of lanthanum metal-organic frameworks (La-MOFs) as degradation photocatalyst of rhodamine-B, AIP Conf. Proc. 2242 (2020) 1–8, https://doi.org/10.1063/5.0013010.

[48] A. Zulys, A. Adawiah, J. Gunlazuardi, M. Derry, L. Yudhi, Light-Harvesting metal-organic frameworks (MOFs) La-ptc for photocatalytic dye degradation, Bull. Chem. React. Eng. Catal. 16 (2021) 170–178, https://doi.org/10.9767/bcrec.16.1.10309.